Reduced North Atlantic Central Water formation in response to early Holocene ice-sheet melting

Audrey Bamberg,[1,2] Yair Rosenthal,[3] André Paul,[1] David Heslop,[1] Stefan Mulitza,[1] Carsten Rühlemann,[2] and Michael Schulz[1]

Received 5 May 2010; revised 5 July 2010; accepted 26 July 2010; published 10 September 2010.

[1] Central waters of the North Atlantic are fundamental for ventilation of the upper ocean and are also linked to the strength of the Atlantic Meridional Overturning Circulation (AMOC). Here, we show based on benthic foraminiferal Mg/Ca ratios, that during times of enhanced melting from the Laurentide Ice Sheet (LIS) between 9.0–8.5 thousand years before present (ka) the production of central waters weakened the upper AMOC resulting in a cooling over the Northern Hemisphere. Centered at 8.54 ± 0.2 ka and 8.24 ± 0.1 ka our dataset records two ~150-year cooling events in response to the drainage of Lake Agassiz/Ojibway, indicating early slow-down of the upper AMOC in response to the initial freshwater flux into the subpolar gyre (SPG) followed by a more severe weakening of both the upper and lower branches of the AMOC at 8.2 ka. These results highlight the sensitivity of regional North Atlantic climate change to the strength of central-water overturning and exemplify the impact of both gradual and abrupt freshwater fluxes on eastern SPG surface water convection. In light of the possible future increase in Greenland Ice Sheet melting due to global warming these findings may help us to better constrain and possibly predict future North Atlantic climate change. **Citation:** Bamberg, A., Y. Rosenthal, A. Paul, D. Heslop, S. Mulitza, C. Rühlemann, and M. Schulz (2010), Reduced North Atlantic Central Water formation in response to early Holocene ice-sheet melting, *Geophys. Res. Lett.*, *37*, L17705, doi:10.1029/2010GL043878.

1. Introduction

[2] Recent oceanographic observations indicate that the AMOC in the North Atlantic (Figure 1) is linked to internal dynamics of the North Atlantic Subpolar Gyre (SPG) on multidecadal timescales [*Hatun et al.*, 2005]. The strong variability of the SPG appears to influence the pathway and northern access of warm and saline surface waters to AMOC convection sites in the Nordic seas and thus directly affects deepwater production. Similarly SPG dynamics control the relative amount of polar and subtropical surface waters available for the formation of subpolar mode waters (SPMW), south of Iceland and east of 25°W (Figure 1). Surface densities of SPMW range between $\sigma_{\Theta} =$ 27.3 to 27.6 [*Levitus*, 1989; *McCartney and Talley*, 1982] and their subduction and subsequent southward flow along these density surfaces as Eastern North Atlantic Central Waters (ENACW) along the Northwest African coastline is well established [*Keffer*, 1985; *Levitus*, 1989; *McCartney and Talley*, 1982; *McDowell et al.*, 1982]. After ~30°N ENACW turn southwestward into the southern STG. ENACW thus establishes a direct link between both gyres in the North Atlantic and provides the opportunity to infer past and present changes in North Atlantic variability. However, our understanding of this intermediate-depth or upper overturning branch of the AMOC and its role in Northern Hemisphere climate variability is limited since it has so far been underrepresented in numerical and paleoclimate investigations. Notable exceptions are *Slowey and Curry* [1995], who focus on glacial/interglacial changes of thermocline ventilation in the western boundary of the STG and *Talley* [2003] who presented a global summary of modern, shallow intermediate and deep overturning regimes. The importance and role of central water overturning and southward export of these water masses into the STG during the Holocene were however not discussed in detail in these studies.

[3] There is increasing consensus that a direct link exists between an increased freshwater flux to the North Atlantic and the weakening of the AMOC [*LeGrande et al.*, 2006; *Renssen et al.*, 2001]. However, most paleo- and numerical reconstructions focus on the deep branch of the AMOC, its response to a freshwater forcing and its influence on glacial and future climate change. Therefore it remains unclear, by what mechanism increased melting and atmospheric forcing affect the upper limb of the AMOC, how such a signal is transferred from surface to central waters, and how these changes affect North Atlantic climate change. Here we investigate the response of the upper limb of the AMOC (central/intermediate water) to increased melting of the LIS during the early Holocene. Enhanced freshwater discharges between 9.0 and 8.0 ka resulted from the demise of continental ice sheets [*Koerner and Fisher*, 1990; *Teller et al.*, 2002] and collapses of proglacial lakes. The final drainage of Lake Agassiz/Ojibway at 8.47 ± 0.3 ka was the largest (~1.63×10^{14} m^3 of freshwater [*Teller et al.*, 2002], equivalent to a 0.4–1.2 m sea level rise [*Cronin et al.*, 2007]) and has thus often served as an example to investigate the abrupt response of the AMOC to future meltwater inputs even though the volume and lake discharge rates were much greater than high-end estimates for future global sea level rise of 0.55 to 1.25 cm yr^{-1} [*Rahmstorf*, 2007]. Indeed, recent high resolution studies focusing on the abrupt cooling episode of the 8.2 ka event, successfully demonstrated the sensitivity of lower North Atlantic Deep Water (LNADW)

[1]MARUM Center for Marine Environmental Sciences and Faculty of Geosciences, University of Bremen, Bremen, Germany.
[2]Federal Institute for Geosciences and Natural Resources, Hannover, Germany.
[3]Institute for Marine and Coastal Sciences and Department of Geology, Rutgers University, New Brunswick, New Jersey, USA.

0094-8276/10/2010GL043878

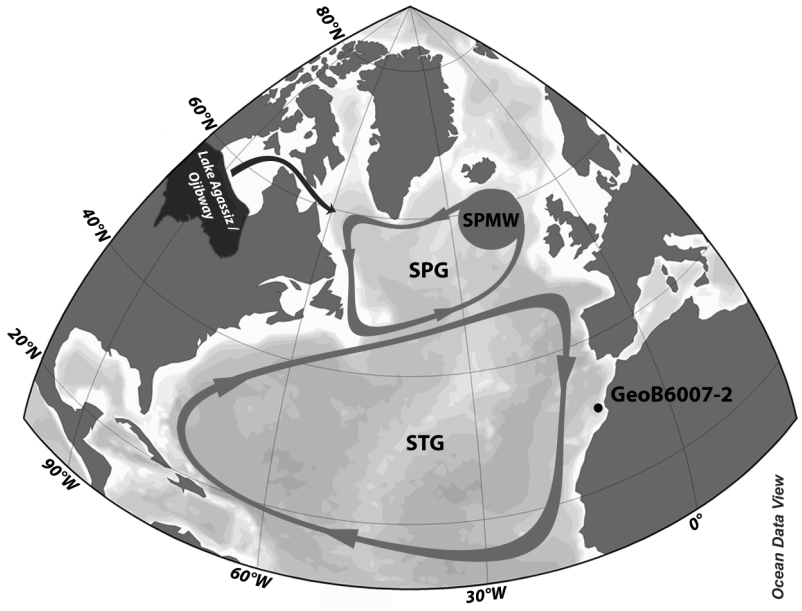

Figure 1. Study area: the location of core GeoB6007-2 (30.85 °N, 10.27 °W at 899 m depth) marked by a black circle. Simplified SPG and STG positions and circulation patterns are indicated by grey loops. The formation region of SPMW is marked by a circle between ~50-63 °N east of 25°W [*Levitus*, 1989; *McCartney and Talley*, 1982]. The total area of Lake Agassiz/Ojibway is shaded in gray and the general pathway of the lake drainage into the polar North Atlantic is marked by a dark arrow modified after *Teller et al.* [2002].

formation to the lake drainage [*Ellison et al.*, 2006; *Kleiven et al.*, 2008] and thereby support climate models that predict a decrease in the lower limb of the AMOC associated with a climate cooling [*LeGrande et al.*, 2006; *Renssen et al.*, 2001] in response to the lake drainage. However, numerous climate archives across the Northern Hemisphere also record a broad interval of climate deterioration starting at ~9.0 ka, well before the drainage of Lake Agassiz/Ojibway [*Alley and Ágústsdóttir*, 2005; *Rohling and Pälike*, 2005]. By analysing the response of the upper limb of the AMOC to both the background melting and lake drainage, we examine whether the increased background melting predating the proglacial lakes' burst is associated with a reduction of the upper AMOC, and if so, whether the broad cooling interval from 9.0 to 8.5 ka is a useful analogue to understanding future mechanisms associated with the possible increase in GIS melting.

2. Oceanographic Setting

[4] Sediment core GeoB6007-2 (30.85 °N, 10.27 °W at 899 m depth) retrieved off Cape Ghir (Figure 1) provides the basis for our analysis. High average sedimentation rates of 70 cm kyr^{-1} (see Figure S1 and Table S1 of the auxiliary material for GeoB6007-2 age model) resulting from high terrigenous input and extensive local productivity ensure high resolution paleoclimate reconstructions.[1] The Cape Ghir upwelling filament leads to high organic-matter fluxes over the core site that create strong and stable local eutrophic conditions [*Eberwein and Mackensen*, 2006]. Thus under constant oxygen content, down-core $\delta^{13}C$ values from infaunal benthic foraminifer should correlate systematically with past organic carbon fluxes [*Schmiedl et al.*, 2004]. At 900 m depth 8.3 °C and 35.2 p.s.u [*Levitus*, 2001], the dominant bottom water mass at the core site originates from northern ENACW [*Knoll et al.*, 2002].

[5] We reconstructed temperature and the oxygen-isotopic composition of seawater ($\delta^{18}O_{sw}$), which is a proxy for paleosalinity using paired Mg/Ca – $\delta^{18}O$ on the shallow infaunal benthic foraminifera *Hyalinea balthica* (see Figure S2 and Table S2). Additionally, $\delta^{18}O_{sw}$ values were calculated using a quadratic paleotemperature equation [*Shackleton*, 1974], and paleosalinities were estimated using modern $\delta^{18}O_{sw}$ – salinity relationships (Figure S3). Additionally, we used carbon isotopes ($\delta^{13}C$; *H. balthica*) as a paleoproductivity proxy to trace past changes in local upwelling intensity [*Schmiedl et al.*, 2004].

3. Reconstructing Hydrography

[6] The isotopic oxygen and carbon compositions ($\delta^{18}O$ and $\delta^{13}C$) of the foraminiferal shells were measured using a Finnigan MAT 251 mass spectrometer equipped with an automatic carbonate preparation device and reported against Vienna PDB (VPDB). Internal precision, based on replicates of a limestone standard, was better than ± 0.07 ‰. Up to 25 *H. balthica* tests from the 250–350 μm size fraction were analyzed for Mg/Ca ratios, using a modified reductive, oxidative cleaning [*Barker et al.*, 2003] and analyzed at Rutgers Inorganic Analytical Laboratory (RIAL) using a Sector Field Inductively Coupled Plasma Mass Spectrometer (Thermo Element XR) following the methods outlined by *Rosenthal et al.* [1999]. The long-term analytical precision of Mg/Ca ratios is based on three consistency standards of Mg/Ca concentrations of 1.10, 2.40 and 6.10 mmol mol^{-1}. Over the course of this study the precision for the consistency standards was 1.6, 1.2 and 1.2 % (residual standard

[1]Auxiliary materials are available in the HTML. doi:10.1029/2010GL043878.

deviation) respectively. Shell weights showed no dissolution effect. For paleotemperature reconstructions the equation Mg/Ca = 0.44T (°C) + 0.52 was used (see Figures S2 and S3 and Table S2). Standard error estimates for paleotemperature, $\delta^{18}O_{sw}$ and salinity values are ± 0.70 °C, ± 0.32 ‰ and ± 0.69 psu, respectively. To calculate these values we followed standard error propagation calculations for a quadratic paleotemperature equation [*Shackleton*, 1974] (see Text S1, section 2), including measurement and calibration errors, uncertainties in the freshwater end-member of the modern $\delta^{18}O_{sw}$ - S relationship, and uncertainties in estimates for global ice-volume changes. We assumed a constant $\delta^{18}O_{sw}$ - S relationship for down-core salinity reconstructions.

4. Early Holocene Cooling

[7] The cooling (~1 °C/500 years) and freshening (~0.3 ‰/500 years) trends observed in the central/intermediate water temperature and $\delta^{18}O_{sw}$ records between 9.0 and 8.5 ka (Figure 2) indicate that freshening and cooling of ENACW occurred well before the collapse of Lake Agassiz/Ojibway. The presence of a broad multi-century background cooling anomaly over the North Atlantic region prior to the drainage of Lake Agassiz/Ojibway is also recorded in numerous other Northern hemisphere records [e.g., *Rohling and Pälike*, 2005]. During this interval, orbitally induced insolation, summer melt rates in the Canadian high Arctic and freshwater export from the remnant Northern Hemisphere ice sheets, in particular the LIS, were enhanced and resulted in rapid surface ocean freshening and a sea level rise of 6.6 ± 0.8 m at a rate of ~1.3 cm yr^{-1} [*Carlson et al.*, 2008; *Cronin et al.*, 2007; *Koerner and Fisher*, 1990]. While an increase in insolation may thus favor melting of northern ice sheets by warmer summer time temperatures in high latitudes, the resulting freshwater input effectively cooled and freshened the surface ocean in the North Atlantic region. Further, our results imply a decrease in surface water density south of Iceland due to declining salinity values between 9.0 and 8.5 ka (Figure S4). The freshening resulted in lighter surface water over ENACW formation sites and thus weakening of regional winter convection and cooling in response to the persistent background melting prior to the drainage of Lake Agassiz/Ojibway between 9.0 and 8.5 ka.

[8] The increase in potassium concentrations in the GISP2 ice core record (Figure 3) between 9.0 and 8.5 ka [*Mayewski et al.*, 1997] suggests that the influence of the polar atmospheric vortex was also strengthening during this period [*Rohling and Pälike*, 2005]. Today, an augmented stratospheric circulation strengthens the positive mode of the Arctic Oscillation [*Baldwin and Dunkerton*, 1999; *Shindell et al.*, 2001], augments the vigor and size of the SPG [*Häkkinen and Rhines*, 2004], and thus the export of fresher and cooler subpolar waters to the SPMW formation region in the eastern SPG. Assuming this link can be applied to longer timescales, a stronger polar vortex would also have led to an intensification of the Trade Winds. This is in line with enhanced local upwelling off Northwest Africa during the early Holocene [*deMenocal et al.*, 2000]. Accordingly, we propose that an increase in upwelling and thus higher local primary productivity between 9.0 and 8.0 ka resulted in higher carbon rain rates over the core site. The decomposition of organic matter causes steeper $\delta^{13}C$ dissolved inorganic carbon gradients in surface sediments, and thus lighter $\delta^{13}C$ values [*Schmiedl et al.*, 2004] are recorded by infaunal benthic foraminifera communities. The significant co-variation between the three intermediate water proxy records demonstrates that lighter $\delta^{13}C$ values correlate with the formation of colder ($r = 0.35$, $p < 0.01$, $n = 53$) and fresher ($r = 0.57$, $p < 0.0001$, $n = 52$) ENACW and thus as discussed above, with a reduced upper AMOC limb.

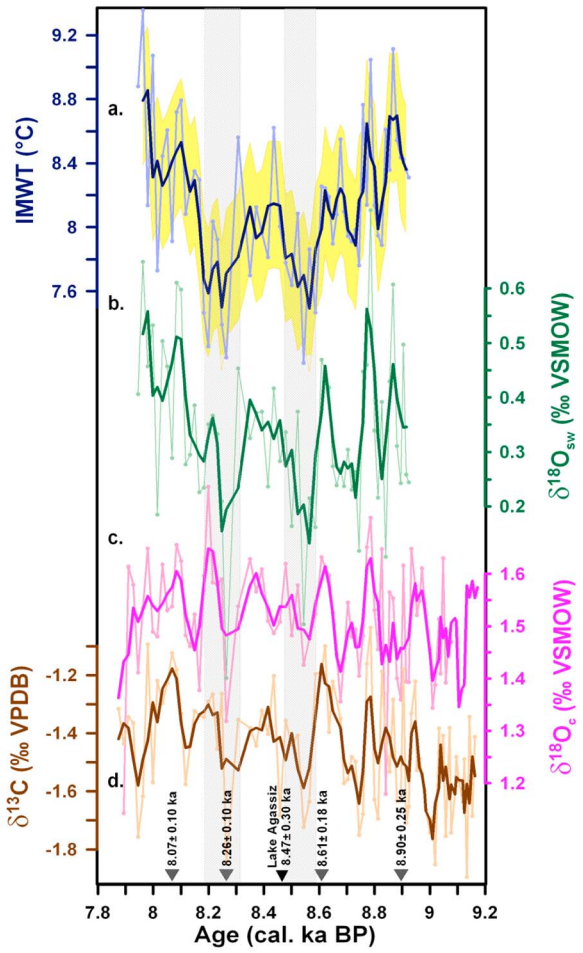

Figure 2. Proxy records from GeoB-6007-2: (a) Mg/Ca-based intermediate-water temperatures (IMWT) and (b) salinity estimates derived from paired Mg/Ca - $\delta^{18}O$ measurements. Also shown is a scale bar for $\delta^{18}O_{sw}$ values corrected for whole-ocean ice-volume changes. (c and d) show Benthic (*H. balthica*) foraminiferal stable oxygen ($\delta^{18}O_c$ ‰VSMOW) and carbon isotopes ($\delta^{13}C$ ‰ VPDB). All graphs are plotted versus age (for age model see auxiliary material) and three-point running means are shown in bold. Also shown are the error envelopes [*Badger et al.*, 1998] for the temperature reconstructions (for the three-point running mean) and calibrated AMS radiocarbon dates with a ± 2 σ error.

5. Oceanic Response to Lake Agassiz/Ojibway Drainage

[9] Centered at 8.54 ± 0.2 and 8.24 ± 0.1 ka paired Mg/Ca and $\delta^{18}O$ values reveal two abrupt ~150 year long events, each recording a temperature drop of ~0.7 °C and a ~0.3 ‰

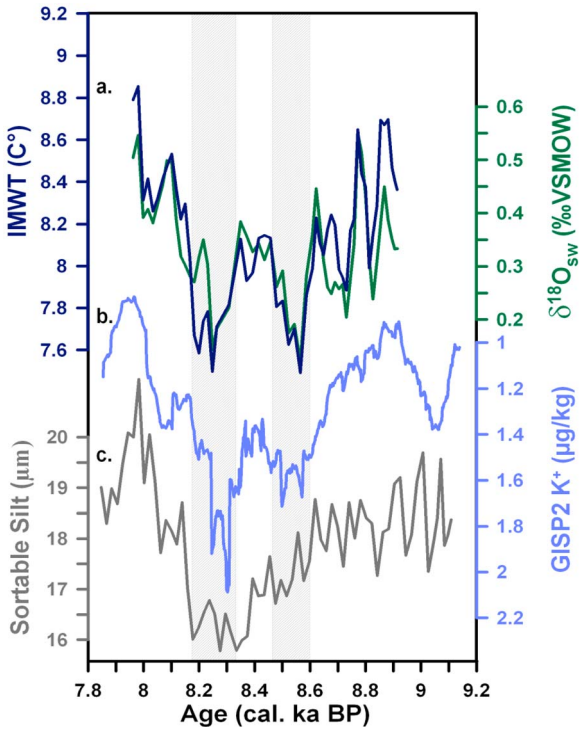

Figure 3. Proxy comparison: the comparison of (a) the three-point running means of the $\delta^{18}O_{sw}$ (‰ VSMOW) and intermediate-water temperature (IMWT) results from GeoB6007-2 with the (b) GISP2 potassium ion record (GISP2 K^+ (μg/kg) and the (c) sortable silt record from core MD99-2251 at 57°27′ N, 27°54′ W [*Ellison et al.*, 2006] illustrate the link between atmospheric and oceanic response to solar variability and background melting.

and ~0.2 ‰ (VSMOW) $\delta^{18}O_{sw}$ decrease, respectively. The first cooling event between 8.46 to 8.61 ka correlates well with the drainage of Lake Agassiz/Ojibway at 8.47 ± 0.3 ka [*Alley and Ágústsdóttir*, 2005]. The abrupt temperature and salinity decreases in our record suggest that melt-waters from the lake drainage rapidly reached ENACW formation sites and thereby further weakened the upper limb of the AMOC. Separated from the first event by a partial recovery of ~200–300 years, the second event at 8.17 to 8.31 ka is concurrent with the maximum cooling observed in the $\delta^{18}O$ GISP2 ice core record as well as with the maximum slowdown of LNADW formation associated with the 8.2 ka event [*Ellison et al.*, 2006; *Kleiven et al.*, 2008] (Figure 3). Further, the combined temperature and salinity values suggest that ENACW density tended towards lighter density surfaces during both 150-year-long events, with lightest values centered at 8.24 and 8.52 ka (Figure S4). The presented data thus suggest that the second event at 8.2 ka resulted from a combined reduction in the upper and lower limbs of the AMOC, whereas the background melting between 9.0 and 8.5 ka and the immediate flood response to the Lake drainage mainly weakened the upper AMOC (Figure 3).

[10] Underlying the entire record, the presented temperature, $\delta^{18}O_{sw}$, and $\delta^{13}C$ data display centennial variability suggesting frequent oscillations and thus the presence of background instabilities in the upper AMOC system. Cross-spectral analysis of the $\delta^{13}C$ record with the INCAL04 ^{14}C dataset [*Reimer et al.*, 2004] indicates significant coherency ($p = 0.05$) at periods of 200 years (Figure S5) supporting a direct link between solar variability and ocean response at central/intermediate water depth. The response of the upper AMOC to these processes may thus explain the presence of the 200–300 year partial recovery between the first and second event and thus further underscores the importance of ocean/atmosphere teleconnections for the upper AMOC and relative regional cooling in the Northern Hemisphere.

6. Summary and Conclusions

[11] The presented central/intermediate water records show that surface-water freshening and cooling are communicated from the SPG into the STG via decreased central/intermediate water ventilation of the upper AMOC limb. Model simulations suggest that increased greenhouse gases will strengthen the atmospheric polar vortex and the positive phase of the Arctic Oscillation [*Shindell et al.*, 2001]. Similarly to our observations between 9.0 and 8.5 ka, meltwater input into the North Atlantic from the GIS as well as from the predicted increase in Arctic freshwater export [*Dickson et al.*, 2007] may have the potential to weaken the central-water branch of the North Atlantic in the future. The recorded upper AMOC response to increased background melting between 9.0 and 8.5 ka is thus a more realistic analogue for future background melting of the GIS than the combined upper and lower response of the AMOC to the drainage of Lake Agassiz/Ojibway. These results, demonstrating a direct link between surface density in the eastern SPG and central-water circulation, provide us with the opportunity to improve the representation of the upper AMOC in numerical model simulations and allow us to gain new insights on the impact of enhanced meltwater input into the North Atlantic on future regional climate change.

[12] **Acknowledgments.** We thank Jeroen Groeneveld for discussion on the Mg/Ca calibration of *H. Balthica* and for valuable editorial suggestions on the manuscript. Stable isotope analyses were run at the University of Bremen by M. Segl. We would also like to thank T. Babila and the trace-metal geochemistry lab crew at IMCS, Rutgers University. We thank an anonymous reviewer for helpful comments on the manuscript. The research was funded by the Deutsche Forschungsgemeinschaft INTERDYNAMIC DFG-Schwerpunktprogramm 1266 to AB, AP, DH, SM, CR and MS and NSF OCE0902977 to YR.

References

Alley, R. B., and A. M. Ágústsdóttir (2005), The 8k event: Cause and consequences of a major Holocene abrupt climate change, *Quat. Sci. Rev.*, *24*(10–11), 1123–1149, doi:10.1016/j.quascirev.2004.12.004.

Badger, M. R., et al. (1998), The diversity and coevolution of Rubisco, plastids, pyrenoids, and chloroplast-based CO_2-concentrating mechanisms in algae, *Can. J. Bot.*, *76*, 1052–1071, doi:10.1139/cjb-76-6-1052.

Baldwin, M. P., and T. J. Dunkerton (1999), Propagation of the Arctic Oscillation from the stratosphere to the troposphere, *J. Geophys. Res.*, *104*(D24), 30,937–30,946, doi:10.1029/1999JD900445.

Barker, S., M. Greaves, and H. Elderfield (2003), A study of cleaning procedures used for foraminiferal Mg/Ca paleothermometry, *Geochem. Geophys. Geosyst.*, *4*(9), 8407, doi:10.1029/2003GC000559.

Carlson, A. E., et al. (2008), Rapid early Holocene deglaciation of the Laurentide ice sheet, *Nat. Geosci.*, *1*(9), 620–624, doi:10.1038/ngeo285.

Cronin, T. M., P. R. Vogt, D. A. Willard, R. Thunell, J. Halka, M. Berke, and J. Pohlman (2007), Rapid sea level rise and ice sheet response to 8,200-year climate event, *Geophys. Res. Lett.*, *34*, L20603, doi:10.1029/2007GL031318.

deMenocal, P., J. Ortiz, T. Guilderson, and M. Sarnthein (2000), Coherent high- and low-latitude climate variability during the Holocene warm period, *Science*, *288*, 2198–2202, doi:10.1126/science.288.5474.2198.

Dickson, R., et al. (2007), Current estimates of freshwater flux through Arctic and subarctic seas, *Prog. Oceanogr.*, *73*(3–4), 210–230, doi:10.1016/j.pocean.2006.12.003.

Eberwein, A., and A. Mackensen (2006), Regional primary productivity differences off Morocco (NW-Africa) recorded by modern benthic foraminifera and their stable carbon isotopic composition, *Deep Sea Res., Part I*, *53*(8), 1379–1405, doi:10.1016/j.dsr.2006.04.001.

Ellison, C. R. W., et al. (2006), Surface and deep ocean interactions during the cold climate event 8200 years ago, *Science*, *312*(5782), 1929–1932, doi:10.1126/science.1127213.

Häkkinen, S., and P. B. Rhines (2004), Decline of subpolar North Atlantic circulation during the 1990s, *Science*, *304*(5670), 555–559, doi:10.1126/science.1094917.

Hatun, H., et al. (2005), Influence of the Atlantic Subpolar Gyre on the thermohaline circulation, *Science*, *309*(5742), 1841–1844, doi:10.1126/science.1114777.

Keffer, T. (1985), The ventilation of the world's oceans: Maps of the potential vorticity field, *J. Phys. Oceanogr.*, *15*(5), 509–523, doi:10.1175/1520-0485(1985)015<0509:TVOTWO>2.0.CO;2.

Kleiven, H. F., et al. (2008), Reduced North Atlantic Deep Water coeval with the glacial Lake Agassiz freshwater outburst, *Science*, *319*(5859), 60–64, doi:10.1126/science.1148924.

Knoll, M., et al. (2002), The Eastern Boundary Current system between the Canary Islands and the African coast, *Deep Sea Res., Part II*, *49*(17), 3427–3440, doi:10.1016/S0967-0645(02)00105-4.

Koerner, R. M., and D. A. Fisher (1990), A record of Holocene summer climate from a Canadian high-Arctic ice core, *Nature*, *343*(6259), 630–631, doi:10.1038/343630a0.

LeGrande, A. N., et al. (2006), Consistent simulations of multiple proxy responses to an abrupt climate change event, *Proc. Natl. Acad. Sci. U. S. A.*, *103*(4), 837–842, doi:10.1073/pnas.0510095103.

Levitus, S. (1989), Interpentadal variability of temperature and salinity at intermediate depths of the North Atlantic Ocean, 1970–1974 versus 1955–1959, *J. Geophys. Res.*, *94*(C5), 6091–6131, doi:10.1029/JC094iC05p06091.

Levitus, S. (2001), *World Ocean Database and World Ocean Atlas 2001*, Ocean Clim. Lab., Natl. Oceanogr. Data Cent., Silver Spring, Md.

Mayewski, P. A., et al. (1997), Major features and forcing of high-latitude northern hemisphere atmospheric circulation using a 110,000-year-long glaciochemical series, *J. Geophys. Res.*, *102*(C12), 26,345–26,366, doi:10.1029/96JC03365.

McCartney, M. S., and L. D. Talley (1982), The subpolar Mode Water of the North Atlantic Ocean, *J. Phys. Oceanogr.*, *12*(11), 1169–1188, doi:10.1175/1520-0485(1982)012<1169:TSMWOT>2.0.CO;2.

McDowell, S., et al. (1982), North Atlantic potential vorticity and its relation to the general circulation, *J. Phys. Oceanogr.*, *12*(12), 1417–1436, doi:10.1175/1520-0485(1982)012<1417:NAPVAI>2.0.CO;2.

Rahmstorf, S. (2007), A semi-empirical approach to projecting future sea-level rise, *Science*, *315*(5810), 368–370, doi:10.1126/science.1135456.

Reimer, P. J., et al. (2004), INTCAL04 terrestrial radiocarbon age calibration, 0–26 cal kyr BP, *Radiocarbon*, *46*(3), 1029–1058.

Renssen, H., H. Goosse, T. Fichefet, and J.-M. Campin (2001), The 8.2 kyr BP event simulated by a global atmosphere–sea-ice–ocean model, *Geophys. Res. Lett.*, *28*(8), 1567–1570, doi:10.1029/2000GL012602.

Rohling, E. J., and H. Pälike (2005), Centennial-scale climate cooling with a sudden cold event around 8,200 years ago, *Nature*, *434*(7036), 975–979, doi:10.1038/nature03421.

Rosenthal, Y., et al. (1999), Precise determination of element/calcium ratios in calcareous samples using sector field inductively coupled plasma mass spectrometry, *Anal. Chem.*, *71*(15), 3248–3253, doi:10.1021/ac981410x.

Schmiedl, G., et al. (2004), Environmental and biological effects on the stable isotope composition of recent deep-sea benthic foraminifera from the western Mediterranean Sea, *Mar. Micropaleontol.*, *51*(1–2), 129–152, doi:10.1016/j.marmicro.2003.10.001.

Shackleton, N. (1974), Attainment of isotopic equilibrium between ocean water and the benthonic foraminifera genus *Uvigerina*: Isotopic changes in the ocean during the last glacial, *Colloq. Int. CNRS*, *219*, 203–209.

Shindell, D. T., et al. (2001), Northern Hemisphere winter climate response to greenhous gas, ozone, solar and volcanic forcing, *J. Geophys. Res.*, *106*(D7), 7193–7210, doi:10.1029/2000JD900547.

Slowey, N. C., and W. B. Curry (1995), Glacial-interglacial differences in circulation and carbon cycling within the upper western North Atlantic, *Paleoceanography*, *10*(4), 715–732, doi:10.1029/95PA01166.

Talley, L. D. (2003), Shallow, intermediate, and deep overturning components of the global heat budget, *J. Phys. Oceanogr.*, *33*(3), 530–560, doi:10.1175/1520-0485(2003)033<0530:SIADOC>2.0.CO;2.

Teller, J. T., et al. (2002), Freshwater outbursts to the oceans from glacial Lake Agassiz and their role in climate change during the last deglaciation, *Quat. Sci. Rev.*, *21*(8–9), 879–887, doi:10.1016/S0277-3791(01)00145-7.

A. Bamberg, D. Heslop, S. Mulitza, A. Paul, and M. Schulz, MARUM Center for Marine Environmental Sciences, University of Bremen, Klagenfurter Straße, GEO Building, D-28359 Bremen, Germany. (audrey.bamberg@uni-bremen.de)

Y. Rosenthal, Institute for Marine and Coastal Sciences, Rutgers University, 71 Dudley Rd., New Brunswick, NJ 08901-8525, USA.

C. Rühlemann, Federal Institute for Geosciences and Natural Resources, Stilleweg 2, D-30655 Hannover, Germany.

AUXILARY MATERIAL

This file includes:

1. Supplementary chronology
   - Figure S1
2. Supplementary calibration, salinity and error calculation
   - Figure S2 and S3
3. Other
   - Figures S4 and S5
4. References

1. Supplementary chronology:

The age model for GeoB6007–2 (Figure S1) was established based on seventeen accelerator mass spectrometry (AMS) radiocarbon measurements (Leibniz-Laboratory for Radiometric Dating and Stable Isotope Research, Kiel University and The National Ocean Sciences Accelerator Mass Spectrometry Facility (NOSAMS), Woods Hole Oceanographic Institution, see Table S1). Mixed species included the following planktonic foraminifera *G. bulloides*, *G. sacculifer*, *G. calida*, *G. ruber*, *G. falconensis*, *G. rubescens*, *T. quinqueloba*, and *O. universa* [*Kim et al.*, 2007; *Kuhlmann et al.*, 2004]. All raw radiocarbon dates were converted into calendar years with the CALIB 5.0.2 software and the MARINE04 marine calibration dataset [*Stuiver and Reimer*, 1993; *Stuiver et al.*, 1998]. We applied the implicit reservoir age correction (ΔR = 0) for all dates because the precise reservoir correction for Northwest Africa is uncertain[*Kim et al.*, 2007]. Ages between calibrated dates were obtained by linear interpolation. The radiocarbon age at 3 cm depth gives a modern age.

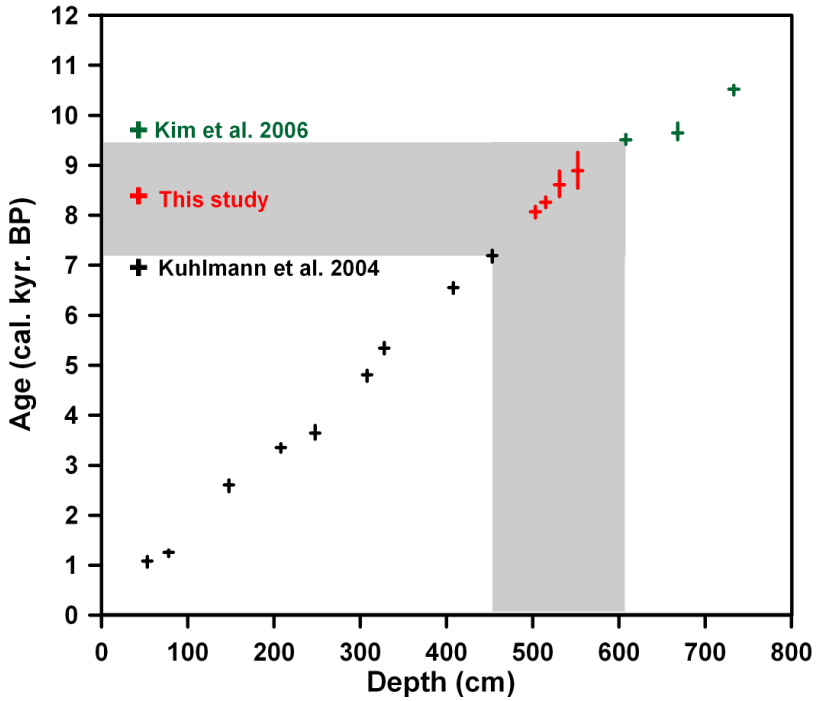

Figure S1: GeobB 6007-2 Age Model. Age-depth relationship of core GeoB6007-2 with focus on the high resolution interval from ca. 450-600 cm.

2. Supplementary calibration, Salinity and error calculation:

***Benthic foraminiferal calibration*:** Intermediate water temperatures were reconstructed from Mg/Ca measurements on the calcitic benthic foraminifer *Hyalinea balthica*, which is a shallow infaunal species living within the top 0.5-1 cm oxygenated, nutrient rich, fine grained sediments [*Eberwein and Mackensen*, 2006; *Schmiedl et al.*, 2000; *Villanueva Guimerans*, 1999] at water depths of ca. 400-1000 m i.e., within ca. 5-14 °C waters [*Morkhoven*, 1986]. A temperature calibration for this species has been obtained using surface sediments from multi-cores collected from the northwest African continental margin during the R/V Meteor Legs M45 and M58 in 1999 and 2002. Core tops used in this calibration are of modern age with relatively high accumulation rates and thus are likely to reflect the modern conditions. *H. balthica* Mg/Ca ratios range from 3.69 to 6.48 mmol mol^{-1} for temperatures between 6.79 and 12.86 °C (Table S2).
Mg/Ca ratios are strongly correlated with bottom water temperature (in °C), and the data are well fit by a straight line ($r=0.96$, $p<0.0001$):

$$Mg/Ca = (0.44 \pm 0.04)\, T + (0.52 \pm 0.37) \qquad (1)$$

An exponential fit to the data ($r = 0.97$) is not significantly better or worse than the linear one (Figure S2):

$$Mg/Ca = 1.90 \pm 0.30\, e^{0.093 \pm 0.015\, T} \qquad (2)$$

Accordingly we use the simpler linear fit for estimating temperatures from Mg/Ca ratios. The standard error of estimate for equation (1) is ±0.31 mmol mol^{-1} which is equivalent to ±0.70°C. The steep slope of equation (1) illustrates the sensitive response of *H. balthica* to temperature changes and thus reduces Mg/Ca errors in terms of reconstructed temperatures, making *H. balthica* an ideal candidate for Holocene temperature reconstructions. For comparison, Marchitto et al. (2007) [*Marchitto*, 2007]and Lear et al. (2002) [*Lear et al.*, 2002] reported standard errors of 2.4°C and 1.7°C on *Cibicidoides pachyderma and Cibicidoides species* respectively. Further, equation (1) is consistent with a global calibration based on core top samples from Indonesia, North Atlantic and Mediterranean Sea sites (*Rosenthal et al., in preparation*), suggesting that temperature is the dominant control on the Mg/Ca composition of *H. balthica* tests. The global calibration suggests that secondary effects of salinity and carbonate ion saturation are insignificant.

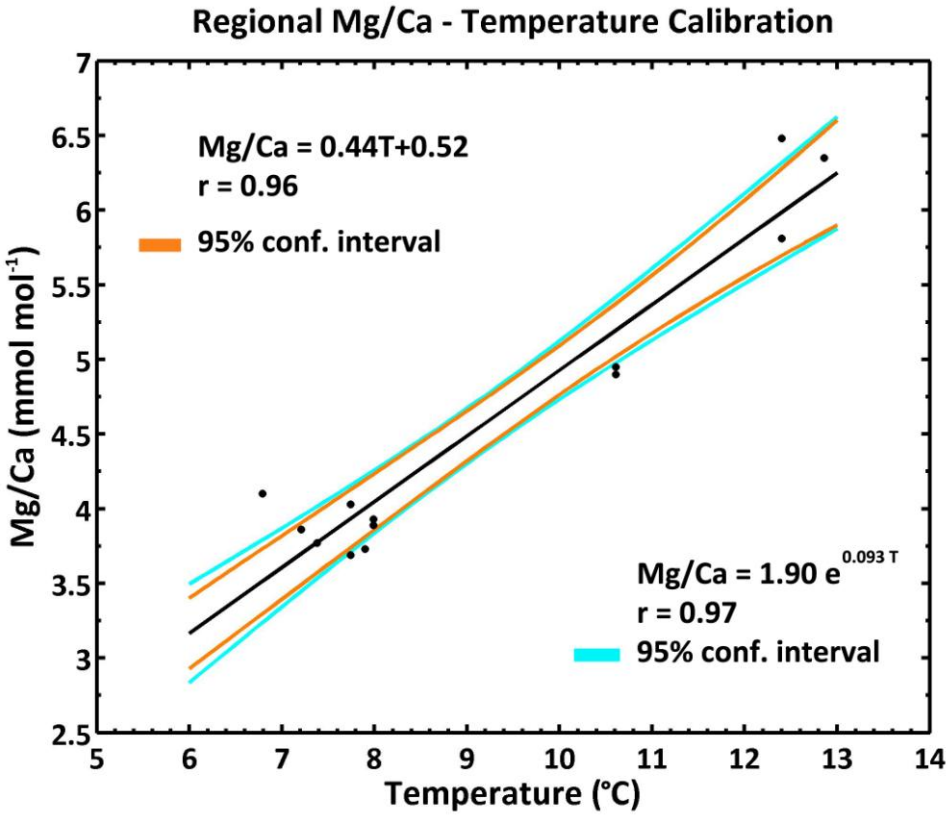

Figure S2: Regional calibration of *H. balthica* (see Table S2). 95 % confidence intervals for the linear (exponential) fit are shown in green (mangenta).

The $\delta^{18}O$ records are based on measurements of *H. balthica* tests. The calibration of NW African core-top samples suggests that the $\delta^{18}O$ composition of the calcitic tests of *H. balthica* follows the expected equilibrium values for calcite with an approximately constant offset of 0.62 ± 0.11 ‰, which is consistent with the 0.64 ‰ offset exhibited by *Cibicidoides* species [*Shackleton and Opdyke*, 1973; *Zahn et al.*, 1986]. Accordingly, the measured $\delta^{18}O$ data on *H. balthica* is corrected for the 0.64 ‰ offset. $\delta^{18}O_{sw}$ values were calculated using a published paleotemperature equation [*Shackleton*, 1974] further corrected for deglacial whole-ocean salinity employing a 120 m sea level rise[*Peltier and Fairbanks*, 2006] and an average ocean depth of 3800 m and a VPDB-to-SMOW $\delta^{18}O$ conversion of 0.27 ‰. The modern water $\delta^{18}O_{sw}$- salinity relationship for the North Atlantic[*LeGrande and Schmidt*, 2006] provides the basis for past and present salinity reconstructions. The calculated salinity values were not corrected for the ice volume effect but taken on the modern salinity scale. The estimated standard deviation for absolute salinity reconstructions[*Schmidt*, 1999] is ±0.69 psu. However, modern calculated salinities fall within ±0.30 psu (Figure S3; except for one outlier). Finally, $\delta^{18}O$ and $\delta^{13}C$ core top records were not found to be significantly correlated at the $\alpha = 0.1$ significance level ($r = 0.26$; $n = 30$; $p < 0.1$).

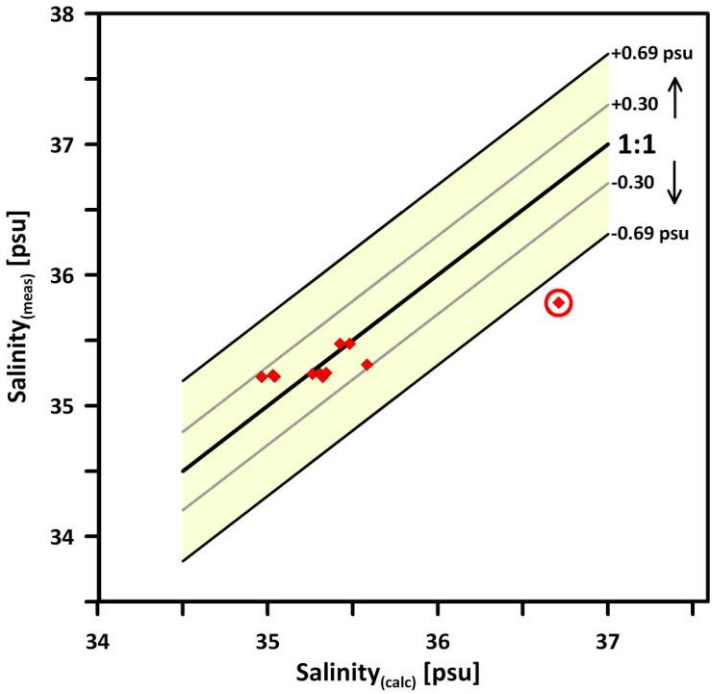

Figure S3: Measured vs. reconstructed Salinity. Calculated salinity values (red dots) fall within ±0.30 psu of the measured core top values except for one outlier. Estimated standard deviations[*Schmidt*, 1999] at ±0.69 and ±0.30 psu are shown in black and grey respectively.

3. Other:

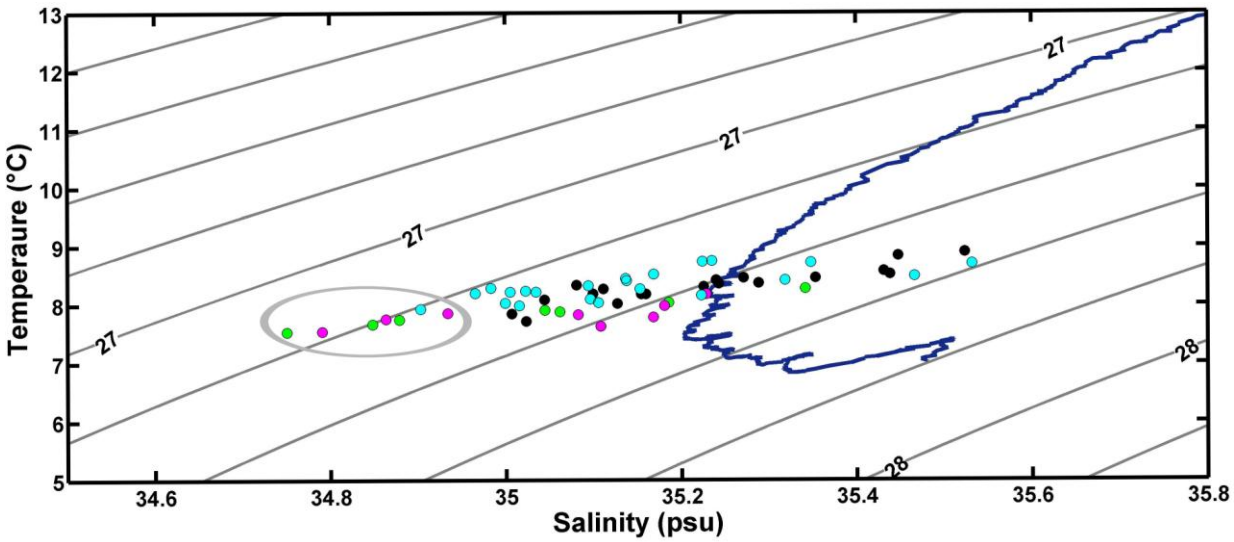

Figure S4: Density Plot: Temperature and Salinity results are plotted along density lines and compared to a local CTD cast (blue) [*Knoll et al.*, 2002]. Data points between 9.0 and 8.5 ka BP are plotted in light blue. The results for events (1) and (2) are shown in green and magenta respectively and the remaining data points are shown in black. The lightest values (within oval) are centered at 8.24 and 8.52 ka BP.

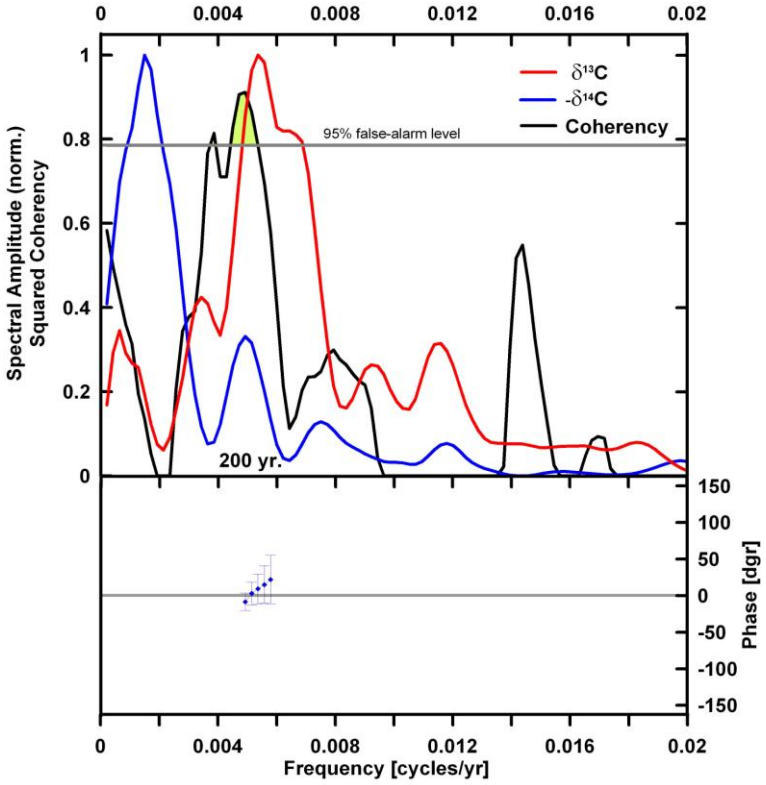

Figure S5: Cross-spectral analysis. Top: Normalized power spectra of $\delta^{13}C$ and negative $\delta^{14}C$ as well as squared coherency between both series. **Bottom:** Phase spectrum between $\delta^{13}C$ and $\delta^{14}C$ (inverted) series indicates no or only slight positive phase lag between both time series. 95 % confidence intervals are only shown if the coherency is significant (p = 0.05; horizontal line indicates false-alarm level for coherency). Analysis carried out with SPECTRUM [*Schulz and Stattegger*, 1997].

4. References:

Eberwein, A., and A. Mackensen (2006), Regional primary productivity differences off Morocco (NW-Africa) recorded by modern benthic foraminifera and their stable carbon isotopic composition, *Deep Sea Research Part I: Oceanographic Research Papers*, *53*(8), 1379-1405.

Kim, J.-H., et al. (2007), Impacts of the North Atlantic gyre circulation on Holocene climate off northwest Africa, *Geology*, *35*(5), 387-390.

Knoll, M., et al. (2002), The Eastern Boundary Current system between the Canary Islands and the African Coast, *Deep Sea Research Part II*, *49*(17), 3427-3440.

Kuhlmann, H., et al. (2004), The transition of the monsoonal and the N Atlantic climate system off NW Africa during the Holocene, *Geophysical Research Letters*, *31*(22), L22204.

Lear, C. H., et al. (2002), Benthic foraminiferal Mg/Ca-paleothermometry: a revised core-top calibration, *Geochimica et Cosmochimica Acta*, *66*(19), 3375-3387.

LeGrande, A. N., and G. A. Schmidt (2006), Global gridded data set of the oxygen isotopic composition in seawater, *Geophys. Res. Lett.*, *33*(12), L12604.

Marchitto, T. M., Bryan, S. P., Curry, W. B. and McCorkle, D. C. (2007), Mg/Ca temperature calibration for the benthic foraminifer *Cibicidoides pachyderma*, *Paleoceanography*, *22*, 1-9.

Morkhoven, v., F.P.C.M., Berggren, W.A. y Edwards, A.S. (1986), Cenozoic Cosmopolitan Deep-Water Benthic Foraminifera, *Bulletin de Centres de Recherches Exploration-Production Elf-Aquitaine*, *11*, 421.

Peltier, W. R., and R. G. Fairbanks (2006), Global glacial ice volume and Last Glacial Maximum duration from an extended Barbados sea level record, *Quaternary Science Reviews*, *25*(23-24), 3322-3337.

Schmidt, G. A. (1999), Error analysis of paleosalinity calculations, *Paleoceanography*, *14*(3), 422-429.

Schmiedl, G., et al. (2000), Trophic control of benthic foraminiferal abundance and microhabitat in the bathyal Gulf of Lions, western Mediterranean Sea, *Marine Micropaleontology*, *40*(3), 167-188.

Schulz, M., and K. Stattegger (1997), SPECTRUM: Spectral analysis of unevenly spaced paleoclimatic time series, *Comput. Geosci.*, *23*, 929-945.

Shackleton, N. (1974), Attainment of isotopic equilibrium between ocean water and the benthonic foraminifera genus *Uvigerina*: Isotopic changes in the ocean during the last glacial, *Colloq. Int. C.N.R.S.*, *219*, 203-209.

Shackleton, N. J., and N. D. Opdyke (1973), Oxygen isotope and paleomagnetic stratigraphy of equatorial Pacific core V 28-238: Oxygen isotope temperatures and ice volumes on a 10^5 year scale, *Quartenary Research*, *3*, 39-55.

Stuiver, M., and P. J. Reimer (1993), Extended 14C data-base and revised calib 3.0 C-14 age calibration program, *Radiocarbon*, *35*, 215-230.

Stuiver, M., et al. (1998), INTCAL98 radiocarbon age calibration, 24,000-0 cal BP, *Radiocarbon*, *40*(3), 1041-1083.

Villanueva Guimerans, P. a. C. C., J.L. (1999), Distribution of Planorbulinacea (benthic Foraminifera) assemblages in surface sediments on the northern margin of the Gulf of Cadiz, *BOLETÍN. INSTITUTO ESPAÑOL DE OCEANOGRAFÍA*, *15*(1-4), 181-190.

Zahn, R., et al. (1986), Benthic foraminiferal delta 13C and accumulation rates of organic carbon: Uvigerina peregrina group and Cibicidoides wuellerstorfi., *Paleoceanography*, *1*(1), 27-42.